Theory and Electrochemistry of Cytochrome C

Journal:	*The Journal of Physical Chemistry*
Manuscript ID	jp-2017-009174.R1
Manuscript Type:	Article
Date Submitted by the Author:	n/a
Complete List of Authors:	Seyedi, Salman; Arizona State University, Physics M. Waskasi, Morteza; Arizona State University, Chemistry and Biochemistry Matyushov, Dmitry; Arizona State University, Chemistry and Biochemistry

Theory and Electrochemistry of Cytochrome c

Salman S. Seyedi,[†] Morteza M. Waskasi,[‡] and Dmitry V. Matyushov[†,‡ *,]

†*Department of Physics, PO Box 871504, Tempe, AZ 85287-1504*
‡*School of Molecular Sciences, Arizona State University, PO Box 871604, Tempe, AZ 85287-1604*

E-mail: dmitrym@asu.edu

Abstract

Extensive simulations of cytochrome *c* in solution are performed to address the apparent contradiction between large reorganization energies of protein electron transfer typically reported by atomistic simulations and much smaller values produced by protein electrochemistry. The two sets of data are reconciled by deriving the activation barrier for electrochemical reaction in terms of an effective reorganization energy composed of half the Stokes shift (characterizing the medium polarization in response to electron transfer) and the variance reorganization energy (characterizing the breadth of electrostatic fluctuations). This effective reorganization energy is much smaller than each of the two components contributing to it and is fully consistent with electrochemical measurements. Calculations in the range of temperatures between 280 and 360 K combine long classical molecular dynamics simulations with quantum calculation of the protein active site. The results agree with the Arrhenius plots for the reaction rates and with cyclic voltammetry of cytochrome *c* immobilized on self-assembled monolayers. Small effective reorganization energy, and the resulting small activation barrier, is a general phenomenology of protein electron transfer allowing fast electron transport within biological energy chains.

Introduction

Redox proteins participate in metabolic redox reactions of biology and in photosynthetic and respiratory energy chains responsible for the cross-membrane electron transport. The conditions of operation of redox proteins within energy chains require some design trade-offs to accommodate both the small reaction free energies and the need to place bulky cofactors in the chain at sufficiently long distances. The overall rate of protein electron transfer is the product of the Boltzmann factor describing the activation barrier and the electron coupling (tunneling probability) decaying exponentially with the distance between the donor and acceptor.[1–3]

The Marcus theory of electron transfer[4] defines the free energy barrier for electron transfer, $\Delta G^{\dagger}$, in terms of the reorganization energy λ and the reaction free energy ΔG_0

$$\Delta G^{\dagger} = \frac{(\lambda + \Delta G_0)^2}{4\lambda} \qquad (1)$$

For reactions involving small values of ΔG_0, typical for biology,[5] the reorganization energy becomes the most important factor determining the reaction barrier.

It is often assumed that proteins provide a nonpolar environment for electron transfer, blocking the access of highly polar water to the active sites. This view is supported by the low dielectric constant of protein powders ($\sim 2-5$[6,7]) and the low magnitude of the screening factor (effective dielectric constant[8]) required in the Coulomb law to screen the interaction between the charges. However, hydration of the protein causes ionization of the surface groups and their increased mobility.[9] As a result, any active site of a hydrated protein is surrounded by a nearly uniform density of surface charges[10] maintaining the stability of the folded protein in solution and allowing its solubility in water.[11] While these charges mostly do not affect the electrostatic screening inside the protein, their motions, caused by thermally activated elastic deformations of the protein, produce a significant electrostatic noise at the protein active site.[12] It is this electrostatic noise that affects the electronic energy levels of the donor and acceptor, bringing them into resonance for electron tunneling.[4]

The reorganization energy in the Marcus equation (eq 1) is both the measure of the change in the distribution of charges (polarization) in the medium caused by transferring the electron (nominator in eq 1) and the measure of the breadth of electrostatic fluctuations caused by thermal agitation (denominator in eq 1).[7,12] The Boltzmann factor $\exp[-\Delta G^{\dagger}/(k_{\mathrm{B}}T)]$ then becomes a Gaussian distribution of the variable ΔG_0 with the mean $-\lambda$ and the variance $2k_{\mathrm{B}}T\lambda$.

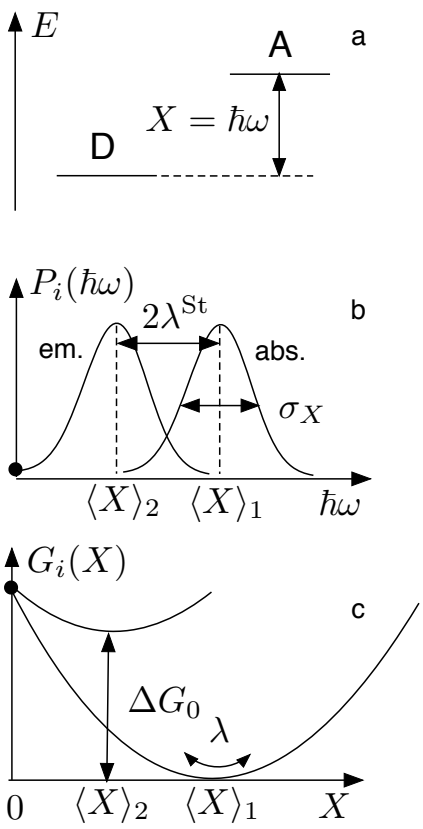

Figure 1: (a) Reaction coordinate $X = \hbar\omega$ for solution electron transfer between the donor (D) and acceptor (A).[13] (b) Probability densities for absorbing (abs.) and emitting (em.) a photon in a charge-transfer optical transition; $\langle X\rangle_i$ stand for the average transition energies. The separation between the peaks of optical transitions represents the Stokes shift and the corresponding reorganization energy $\lambda^{\rm St}$. (c) The free energy surfaces of electron transfer $G_i(X) = G_0^i - k_{\rm B}T\ln[P_i(X)]$ following from the optical transition probabilities $P_i(X)$. The reorganization energy λ defines the curvature of the free energy surface near the bottom (shown by the double arrow). It also provides the measure of inhomogeneous broadening of the optical charge-transfer band[14] ($\sigma_X^2 = \langle(\delta X)^2\rangle = 2k_{\rm B}T\lambda$ in (b) and in eq 3). The filled dots in (b) and (c) indicate, respectively, $P_2(0)$ and the crossing point of $G_i(X)$ representing the transition state, $X = 0$, of the electron-transfer reaction.

Given that a hydrated protein is a soft medium possessing a large density of charge at the protein-water interface, it is hardly a surprise that atomistic computer simulations consistently show large reorganization energies for electron transfer, $\lambda \simeq 1-2$ eV,[15–18] or even higher[19,20] when the simulation trajectories are sufficiently long. More surprising was the realization that the reorganization energy characterizing the fluctuations of the energy levels (thermal agitation) was distinct from the reorganization energy characterizing their shift upon electron transfer (medium polarization).[19] We denote the former, which we call the variance reorganization energy, with the standard Marcus notation λ and the latter with the "Stokes-shift" reorganization energy[21] $\lambda^{\rm St}$. The reason for the latter assignment is that $\lambda^{\rm St}$, characterizing the shift in average energies, is half of the Stokes shift separating the maxima of absorption and emission charge-transfer bands[22,23] (Figure 1).

The typical phenomenology of electrostatic fluctuations at active sites of proteins as calculated from atomistic simulations is the inequality[12,19] $\lambda \gg \lambda^{\rm St}$. The reason for this result can be traced to the non-Boltzmann (non-ergodic) sampling of the phase-space available to the protein on the reaction time-scale,[21] polarizability of the active site,[24,25] or the combination of both these factors and/or some other reasons not yet identified. This phenomenology, as well as some analytic models allowing non-Gaussian fluctuations affecting electron transfer,[24,26,27] provides an extension of the standard Gaussian picture of the Marcus model,[28] which stipulates[29] $\lambda^{\rm St} = \lambda$. At least some of these extensions[24] require non-parabolic free energy surfaces. Since our simulations do not provide sufficient sampling to distinguish such features, the phenomenology of equal-curvature parabolas[21] is used here. Specifically, the variance reorganization energies in the oxidized and reduced states are considered to be equal (given by λ) and distinct from $\lambda^{\rm St}$. This phenomenological approach allows us to accommodate both the non-Boltzmann (non-equilibrium) sampling and polarizability effects (requiring non-parabolic free

energy surfaces[24]) in terms of only two reorganization parameters, λ and $\lambda^{\rm St}$.

Large values of the reorganization energies appearing in simulations come in direct contradiction to often small, in the range $0.3 - 0.6$ eV[30–36] (or even smaller, < 0.25 eV[37,38]), values of the reorganization energy reported by electrochemistry of redox proteins. Since electrostatics is not much sensitive to the details of force fields employed by atomistic simulations, the problem cannot be simply related to still existing deficiencies of the atomistic force-field models. Here we argue that the reorganization energy reported by electrochemistry of proteins is an effective "reaction" (superscript "r") reorganization energy combining two reorganization energies typically reported by simulations

$$\lambda^r = \frac{(\lambda^{\rm St})^2}{\lambda} \qquad (2)$$

The notion that proteins are characterized by the condition $\lambda \gg \lambda^{\rm St}$ explains why relatively small values of λ^r are reported by electrochemical measurements. We derive the equation for the activation barrier, from which the expression for λ^r follows, in eqs 5–8 below. Suffice it to say here that λ^r in the form of eq 2 is a direct consequence of the parabolic shape of the free energy surfaces of electron transfer. One comes back to the standard Marcus picture with $\lambda^r = \lambda = \lambda^{\rm St}$ when $\lambda^{\rm St} = \lambda$.

In order to show the consistency of our theoretical model with experimental data, we have performed extensive simulations of a much studied[39,40] heme protein cytochrome c (Cyt-c, wild type from horse). We show that the temperature dependence of the reaction reorganization energy $\lambda^r(T)$ is consistent with the Arrhenius plots for electrochemical rates obtained from cyclic voltammetry.[33] We also show that the distribution of the energy levels (density of states) of the oxidized heme, caused by thermal agitation of the bath, is consistent with the corresponding distribution obtained by taking the derivative of the cathodic current with the overpotential, $di_c/d\eta$. The cathodic current i_c is obtained from cyclic voltammetry after correction for mass transport.[30,31,41,42] We report an overall good agreement between experiment[30,33,34,43] and the combined application of the analytic theory and computer simulations.[21,25]

Producing reliable values of reorganization parameters of Cyt-c has required the combination of long trajectories of classical molecular dynamics (MD) simulations with quantum calculations of the heme's active site. Since long simulation times are required for the convergence of the reorganization energies, our quantum calculations are based on Warshel's empirical valence-bond method,[44,45] which involves diagonalizing the quantum Hamiltonian, affected by fluctuating electrostatics, along the MD trajectory.[16,25] This specific form of a general QM/MM methodology[46] allows one to combine long trajectories required for sufficient sampling of electrostatic fluctuations with a large number, $M \simeq 100$, of excited quantum states of the active site. These excited states are coupled to the fluctuating electrostatic field through a set of transition dipoles and thus allow us to account for the polarizability of the active site and the corresponding deformation of the electronic density in response to the medium fluctuations.[16,24,25] This part of the calculation formalism turns out to be very essential for achieving low values of λ^r consistent with experiment.

Methods

Theoretical formalism. Modern theories of electron transfer assign the energy gap X between the donor and acceptor energy levels to the electron-transfer reaction coordinate.[13,24,28,29] For electron transfer in solution, one considers the one-electron states of the donor and acceptor and the instantaneous (fluctuating) energy gap X between them as the reaction coordinate. Thermal fluctuations reduce this gap to zero in the activated state of an electron transfer reaction (radiationless transition). The same energy gap comes in resonance with the radiation photon in spectroscopy of charge-transfer transitions (Figure 1a).[47] One observes charge-transfer absorption or emission bands with the maxima corresponding to the

average excitation energies $\langle X\rangle_i$. The separation between the maxima is the spectroscopic Stokes shift,[14,22] which can be used to quantify the reorganization energy labelled as $\lambda^{\rm St}$ (Figure 1b).

If $P_i(\hbar\omega)$ is the probability of absorbing ($i = 1$) or emitting ($i = 2$) a photon with the energy $X = \hbar\omega$, the free energy surfaces of electron are constructed to compliment this picture in terms of the free energy (reversible work) required to achieve a given value of X: $G_i(X) = G_0^i - k_{\rm B}T\ln[P_i(X)]$ (Figure 1c), where G_0^i is the free energy at the minimum. The separation between the minima of the free-energy surfaces then becomes equal to $2\lambda^{\rm St}$. One additionally can define the reorganization energy from the curvature of the free energy surface at the minimum, $\partial^2 G_i(X)/\partial X^2|_{X_{0i}}$, which can be related to the variance of the reaction coordinate X according to the standard rules of statistical mechanics[7,12,29]

$$\lambda = \langle(\delta X)^2\rangle/(2k_{\rm B}T) \qquad (3)$$

Returning to the picture of optical transitions, the variance reorganization energy λ determines the Gaussian width of the energy-gap fluctuations or the inhomogenoues width of a single vibronic optical line.[48] As mentioned above, in the Marcus picture one has $\lambda^{\rm St} = \lambda$, which is a specific case of a general result known as the fluctuation-dissipation theorem.[49] As mentioned above, this phenomenology changes for protein electron transfer in solution, where one finds[12,21] $\lambda \gg \lambda^{\rm St}$.

Electrode electron transfer. In the case of electrode electron transfer, the energy gap involving one-electron states is between the fluctuating energy level of the oxidized reactant in solution $\epsilon_{\rm Ox}$ and the energy level in the metal ϵ (cathodic process, Figure 2).[50] Correspondingly, we replace $i = \{1, 2\}$ for solution electron transfer with $i = \{{\rm Ox}, {\rm Red}\}$ for electrode reactions. While full description of the problem in terms of finite-temperature distribution of the electrons in the metal is possible,[51–55] we first simplify the discussion by considering electron transfer to a single level corresponding to the chemical potential of the electrons in the metal $\mu = \epsilon_F - e\eta$. It is modified by the overpotential η (e is the elementary charge) from the Fermi energy ϵ_F consistent with the equilibrium potential at the electrode (Figure 2).

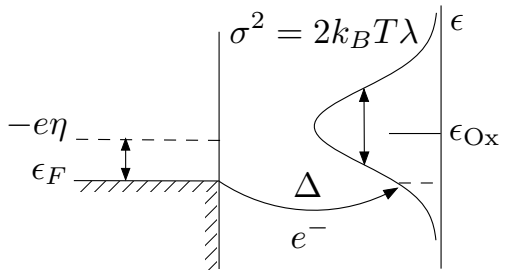

Figure 2: Schematics of cathode electron transfer from the Fermi energy level ϵ_F, corresponding to the equilibrium electrode potential, to an oxidized reactant with the average energy $\epsilon_{\rm Ox}$. Electron transfer predominantly occurs from ϵ_F to a nonequilibrium energy level in resonance with. The electrode-reactant electronic coupling Δ characterizes the tunneling probability (eq 10). The nonequilibrium energy level is a part of a Gaussian manifold with the variance $\sigma^2 = 2k_BT\lambda$ specifying the reorganization energy λ (eq 3). The overpotential η shifts the electrode chemical potential as $\mu = \epsilon_F - e\eta$.

In this picture, the initial state of the system with the electron in the metal is $E_{\rm g}^{\rm Ox} + \mu$, where $E_{\rm g}^{\rm Ox}$ is the ground state of the oxidized state of the reactant. The final state, before any relaxation of the nuclear subsystem has occurred, is the ground quantum state in the reduced state $E_{\rm g}^{\rm Red}$. Both energies refer to the same nuclear configuration of the thermal bath. The electron-transfer reaction coordinate, monitoring the transition to the activation state $X = 0$, is the energy gap between the initial and final states[13,29]

$$X = E_{\rm g}^{\rm Ox} - E_{\rm g}^{\rm Red} + \mu \qquad (4)$$

A generic Gaussian distribution of the reaction coordinate X results in the parabolic free energy surface[12,28,56]

$$G_i(X) = G_0^i + \frac{(X - \langle X\rangle_i)^2}{4\lambda} \qquad (5)$$

where $i = {\rm Ox}, {\rm Red}$.

We can apply the condition of crossing at zero energy gap, $G_{\rm Red}(0) = G_{\rm Ox}(0)$, to obtain the

average values

$$\langle X\rangle_{\rm Ox} = -\lambda^{\rm St} - (\lambda/\lambda^{\rm St})\Delta G_0$$
$$\langle X\rangle_{\rm Red} = \lambda^{\rm St} - (\lambda/\lambda^{\rm St})\Delta G_0 \quad (6)$$

where $\Delta G_0 = G_0^{\rm Red} - G_0^{\rm Ox}$ is the reaction free energy. The Stokes-shift reorganization energy from these equations is half of the separation between the minima of the crossing parabolas

$$\lambda^{\rm St} = \tfrac{1}{2}\left|\langle X\rangle_{\rm Red} - \langle X\rangle_{\rm Ox}\right| \quad (7)$$

The activation barrier for the cathodic process is the free energy difference between the activated state, $G_{\rm Ox}(0)$, and the free energy at the minimum, $G_0^{\rm Ox}$: $\Delta G^\dagger = G_{\rm Ox}(0) - G_0^{\rm Ox}$. One gets from eqs 5 and 6

$$\Delta G^\dagger = \frac{(\lambda^r + \Delta G_0)^2}{4\lambda^r} \quad (8)$$

where λ^r is the effective reorganization energy given by eq 2. Since the reduction and oxidation rates are equal at $\eta = 0$, $e\eta = \Delta G_0$ for the electrochemical discharge. One therefore gets for the barrier of electrochemical electron transfer

$$\Delta G^\dagger = \frac{(\lambda^r + e\eta)^2}{4\lambda^r} \quad (9)$$

The significant result of this derivation is that accepting two equal-curvature parabolas, even with the variance reorganization energy distinct from the Stokes reorganization energy, does not alter the basic Marcus result[4] for the dependence of the activation barrier on the reaction free energy. The two reorganization energies, λ and $\lambda^{\rm St}$, combine into an effective reorganization energy λ^r (eq 2), which is the only parameter that can be reported from experiments altering either the reaction free energy (solution reactions) or the electrode overpotential (electrochemical kinetics). In contrast, spectroscopy of charge-transfer bands allows one to distinguish between $\lambda^{\rm St}$ and λ.[22,23] The former parameter determines the spectroscopic Stokes shift, while the latter yields the inhomogeneous broadening of the spectral lines (Figure 1b).[14,48,57]

The arguments presented here can be extended to the calculation of the rate of nonadiabatic electron transfer, which involves summation of the Golden Rule transitions to all energy levels of the metal below the chemical potential μ. The resulting cathodic rate is[51,58–60]

$$k_c(\eta) = \frac{\Delta}{\hbar}{\rm erfc}\left(\frac{\lambda^r + e\eta}{\sqrt{4k_BT\lambda^r}}\right) \quad (10)$$

where ${\rm erfc}(x)$ is the complimentary error function and $\Delta = \pi\rho_F V^2$ is the electronic coupling between the redox species and the electrode. It is given in terms of the coupling V between the reactant and the individual energy state in the metal and the density of states ρ_F of the conduction electrons at the Fermi level.[52,54,61]

The derivative of the rate over the overpotential, $dk_c/d\eta$, is thus proportional to the "density of states" of the oxidized energy level in the medium

$$P_c(\eta) \propto \exp\left[-\frac{(\lambda^r + e\eta)^2}{4k_BT\lambda^r}\right] \quad (11)$$

This distribution is distinct from the corresponding distribution along the reaction coordinate $P_{\rm Ox}(X) \propto \exp[-\beta G_{\rm Ox}(X)]$ (Figure S2 in SI). The function $P_c(\eta)$ is a measure of the probability $P_{\rm Ox}(0)$ to reach the activated state $X = 0$ when the average $\langle X\rangle_{\rm Ox} = -\lambda^{\rm St} - (e\eta)(\lambda/\lambda^{\rm St})$ is varied by applying the overpotential. The distribution function $P_c(\eta)$ is directly accessible from cyclic voltamemtry upon correction for mass transport.[41]

Solvent dynamics can potentially affect the preexponential factor of the rate constant.[62–65] The rate constant of electron transfer between the electrode and an adsorbed reactant, not affected by diffusion, is given by the following relation[66–68]

$$k_c^s(\eta) = (1+g)^{-1}k_c(\eta) \quad (12)$$

with the nonadiabatic rate constant $k_c(\eta)$ according eq 10. The factor in front of it, correcting for the solvent dynamics, is given by the relation

$$g = \frac{\Delta\langle\tau\rangle}{\hbar}\frac{4k_BT\lambda^r}{(\lambda^r + e\eta)^2} \quad (13)$$

The theory leading to eq 12 is the result of applying the Sumi-Marcus[63] formalism to electrode kinetics.[68] The analytical expressions in

eqs 12 and 13 are obtained under the assumption of a sufficiently low overpotential such that $\lambda^r + e\eta \gg k_B T$.[68] Further, $\langle\tau\rangle$ is the characteristic time of the Stokes-shift dynamics of the energy gap X specified through the energy gap autocorrelation function[69]

$$C_X(t) = \langle \delta X(t) \delta X(0) \rangle \tag{14}$$

where $\delta X(t) = X(t) - \langle X \rangle$ and $\langle\tau\rangle$ is defined as the integral of the normalized time correlation function (average solvation time[70])

$$\langle \tau \rangle = \int_0^\infty dt C_X(t)/C_X(0) \tag{15}$$

The relaxation times in the range $\langle\tau\rangle \simeq 300 - 900$ ps[71–74] were determined from MD simulations (Figure S4 and Table S3 in SI). These Stokes-shift relaxation times were used in eq 13 to estimate the effect of the solvent dynamics on $k_c^s(0)$. It was found to be negligible for the experimental data considered below.

Simulations and data analysis. The NMR solution structure of horse heart cytochrome c (PDB 1GIW) was adopted as the starting configuration for the classical MD simulations. The simulations were done with NAMD software suite,[75] with the trajectory length of ≥ 250 ns for each temperature and oxidation state (overall ≥ 4 μs of MD simulations). The classical MD simulations were followed by empirical valence-bond calculations[44,45] performed for the quantum center including the heme, histidine, methionine, and two cysteine amino acids (Figure 3 and SI) following our protocol developed in the past.[25] The electrostatic potential of the bath $\phi(\mathbf{r})$ acting on the quantum center was expanded around the potential $\phi_{\rm Fe}$ at the heme iron up to the dipolar operator. This expansion leads to a set of transition dipoles $\boldsymbol{\mu}_{jk}^i$ in the matrix of the quantum center Hamiltonian[16,25]

$$H_{jk}^i = \left(E_j^i + Q^i \phi_{\rm Fe}\right) \delta_{jk} - \boldsymbol{\mu}_{jk}^i \cdot \mathbf{E}_b \tag{16}$$

Here, E_j^i is the energy of jth state in either $i =$ Ox or $i =$ Red states and Q^i is the total charge of the quantum center. The excited states j and k are coupled through the electric field of the thermal bath $\mathbf{E}_b$ multiplying transition dipoles $\boldsymbol{\mu}_{jk}^i$ in eq 16. Physically, this term in the Hamiltonian represents the polarization of the heme by the medium field through a nonzero polarizability α_j^i of state j, which is given in terms of the transition dipoles as

$$\alpha_j^i = 2 \sum_{k \neq j} \left|\boldsymbol{\mu}_{jk}^i\right|^2 / \Delta E_{jk} \tag{17}$$

where $\Delta E_{jk} = E_k - E_j$.

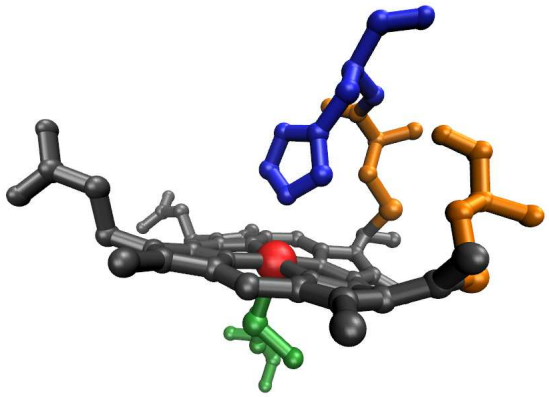

Figure 3: Quantum center of Cyt-c used in the calculations to compute the Hamiltonian matrix in eq 16. It includes the heme (gray, with Fe colored red), histidine (blue), methionine (green), and two cysteine (orange) amino acids.

The quantum states $j = 0, \ldots, M$ include the ground state of the quantum center, $j = 0$, and a number of its excited states produced here by ZINDO/S calculations for the oxidized (Ox, $Q = -1$) and reduced (Red, $Q = -2$) states. The number of states $M = 100$ was chosen to converge the polarizability of the quantum center. Decreasing the number of states M makes the quantum center less polarizable and eventually brings the system back to the Marcus formulation with $\lambda^{\rm St} \simeq \lambda$.[25] Additional details of the simulation protocol and of the quantum calculations are given in the SI.

A polarizable quantum center carrying the polarizability $\boldsymbol{\alpha}^i$ gives rise to the polarization free energy $-(1/2)\mathbf{E}_b \cdot \boldsymbol{\alpha}^i \cdot \mathbf{E}_b$. On the other hand, the free energy (reversible work) invested in creating a fluctuation in the medium scales quadratically with the field,[24,76,77] $(\chi/2)\mathbf{E}_b^2$. The sum of this term and the polarization free

energy lowers the force constant for the medium fluctuation from χ to $\simeq (\chi - \alpha^i)$, $\alpha^i = \frac{1}{3}\mathrm{Tr}[\boldsymbol{\alpha}^i]$. When projected on the reaction coordinate of electron transfer X, less free energy invested in an electrostatic medium fluctuation implies lower curvature of the corresponding parabola $G_i(X)$ and a higher reorganization energy λ.[24] This physical picture is consistent with our simulations.

The Hamiltonian matrix in eq 16 is diagonalized at each instantaneous value of the potential ϕ_{Fe} and the electric field $\mathbf{E}_b$ along the simulation trajectory to produce the minimum eigenvalues $E_{\mathrm{g}}^{\mathrm{Ox/Red}}$ corresponding to the quantum ground state in either oxidized or reduced states of the active site. They are used in eq 4 to produce the trajectory of the fluctuating variable X. The probability distributions of X calculated in the oxidized and reduced states yield the free energy surfaces of the half reaction $G_i(X)$ (Figure S2 in SI).

The reorganization energies λ^{St} and λ are obtained from, correspondingly, the first and second moments of the variable X. The former is defined in terms of the average energy gap $\langle X \rangle_i$ in the Red and Ox states according to eq 7. The latter is given through the variance, $\lambda_i = \langle (\delta X)^2 \rangle_i / (2k_{\mathrm{B}}T)$, $i = \mathrm{Ox}, \mathrm{Red}$. Significantly longer simulations are required to converge λ_i compared to λ^{St} (Figure S1 in the SI). We find λ_{Ox} and λ_{Red} slightly different even after 250 ns of simulations (Figure 4 and Table S1 in the SI). The values of λ used for the kinetic analysis were therefore obtained by taking the mean of the values in the corresponding redox states, $\lambda = (\lambda_{\mathrm{Ox}} + \lambda_{\mathrm{Red}})/2$ (black circles in Figure 4).

A separate issue is the potential impact of the polarizability of the protein-water solvent on the reorganization energies calculated from simulations. Dielectric continuum models predict that the reorganization energy is proportional to the Pekar factor $c_0 = n_D^{-2} - \epsilon_s^{-1}$,[4] which implies a drop by a factor of about n_D^{-2} in going from a non-polarizable solvent to a polarizable solvent with the refractive index n_D (assuming a high static dielectric constant ϵ_s). This perspective would suggest that the reorganization energies obtained by computer simulations in non-polarizable solvents (TIP3P water in this study) would need to be scaled down to account for the polarizability effects. We have recently address this problem by computer simulations and liquid-state theories.[78,79]

It turns out that microscopic solvation models do not support re-scaling of the reorganization energy according to the rules stipulated by dielectric continuum models. In contrast to those predictions, λ stays nearly constant with increasing n_D^2, or even slightly increases (for polarizable water models), instead of the predicted drop. Given these new results and previous simulations and calculations of the effects of the solvent polarizability on electron transfer,[80,81] it is reasonable to suggest that the reorganization parameters obtained from the present simulations do not need further rescaling. A good agreement with experimental results demonstrated below is another indication that our calculation formalism is robust.

We also note that electron transfer in redox proteins is typically accompanied by small structural changes of the active site[82] and, correspondingly, low reorganization energy of active site vibrations. Estimated values range from $0.05 - 0.09$ eV for Fe-porphins[83] to $0.10 - 0.14$ eV for Zn-porphyrins[84] to $\simeq 0.1$ eV in azurins.[85] This internal reorganization energy is generally split between quantum and classical vibrations. The reorganization energy related to quantum vibrations affects the rates in the Marcus inverted region of electron transfer,[86] which is not typically reached in either the electrochemical experiment or at the typical conditions of redox reactions in biological energy chains. Therefore, only the classical part of the internal reorganization energy can potentially affect these reactions. While the splitting of the reorganization energy between the classical and quantum modes is not known for Cyt-c, the classical part of the internal reorganization energy, remaining after subtracting the quantum component, is expected to be small, within the simulation uncertainties. We therefore do not include the internal reorganization energy in our calculations of the electrode kinetics.

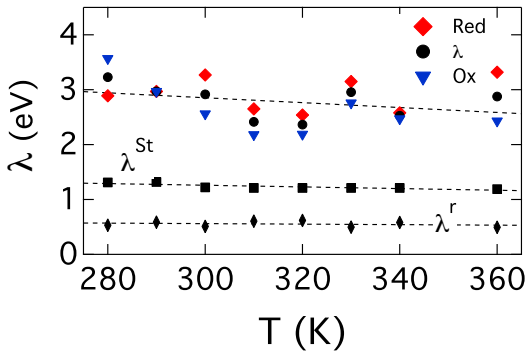

Figure 4: Temperature dependence of reorganization energies from QM/MD simulations. Shown separately are the variance reorganization energies λ_i (eq 3) in the reduced (red diamonds) and oxidized (blue triangles) states of Cyt-c and their mean values (black circles). Squares refer to the Stokes-shift reorganization energy $\lambda^{\rm St}$ (eq 7) and black diamonds refer to the reaction reorganization energy λ^r (eq 2). The dashed lines are linear regressions through the simulation points (the upper dashed line is a linear regression through the mean values $\lambda(T)$).

Results

The results of QM/MD simulations for the reorganization energies as functions of temperature are shown in Figure 4. The corresponding values at $T = 300$ K, estimated from linear regressions of the simulation data, are listed in Table 1. As expected, both reorganization energies, $\lambda^{\rm St}$ and λ, are fairly large and consistent with a large density of charge and polar groups surrounding the active site of a redox protein. A relatively small value of the reaction reorganization energy λ^r (eq 2) is achieved due to $\lambda \gg \lambda^{\rm St}$. As we already pointed out, this inequality in the case of Cyt-c is the consequence of a high polarizability of the active site allowing its electronic density to deform in response to the fluctuations of the thermal bath. Reducing the polarizability by either using fixed partial atomic charges (zero polarizability) or a small number of quantum states when diagonalizing the quantum Hamiltonian produce $\lambda^{\rm St} \simeq \lambda \simeq 1.3 - 1.6$ eV consistent with the standard Marcus picture of a single reorganization energy characterizing electron transfer.[25] However, these values of the reorganization energy are too high to describe the experimental electrochemical data, as we show below.

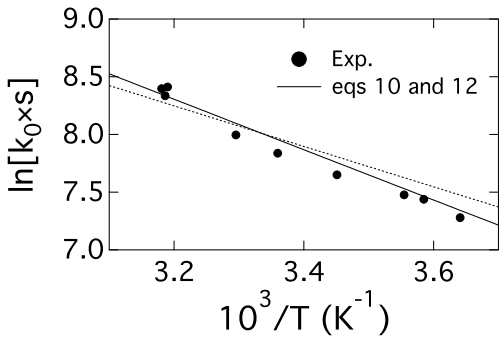

Figure 5: Rate constant $k_0 = k_c(0)$ (eq 10) at $\eta = 0$ for horse Cyt-c on the gold electrode modified with PyC_{11}/C_{10} self-assembled monolayer[33] (points, Exp.). The solid line shows the calculations based on eqs 10 and 12, which give identical results. The electron coupling $\Delta = 2 \times 10^{-9}$ eV is used to reproduce the experimental data. The temperature-dependent reorganization energy $\lambda^r(T)$ from Figure 4 was used in eqs 10 and 12. The dotted line shows the result of neglecting the temperature dependence $\lambda^r(T)$ and putting $\lambda^r = \lambda^r(300\ {\rm K})$.

Not only the reorganization energy itself, but also its temperature dependence is reduced for λ^r compared to $\lambda^{\rm St}$ and λ. We list in Table 1 the entropies of reorganization

$$S_\lambda = -\left(\partial\lambda/\partial T\right)_V \qquad (18)$$

at constant volume consistent with the NVT ensemble used in the simulations (see SI). All reorganization energies are decaying functions with increasing temperature, as is expected from studies of electron-transfer reactions in polar liquids.[87,88]

The decay of the reorganization energy with increasing temperature is related to structural fluctuations in polar liquids producing changes in both orientations of the liquid dipoles and their positions (density fluctuations). While changes in orientations are mostly driven by redistributing the thermal energy (energy driven), the density rearrangements require local repacking of the liquid against repulsive molecular cores (entropy driven). The dif-

ference in the character of fluctuations, energy-driven for rotations and entropy-driven for translations, projects on different effects of temperature on the corresponding components in the reorganization energy. The reorganization energy arising from molecular rotations is nearly temperature-independent, while the reorganization energy arising from density fluctuations decays approximately hyperbolically with increasing temperature. The overall dependence of the reorganization energy on temperature is hyperbolic,[87] as proven experimentally[88,89] for systems with $\lambda^{\rm St} \simeq \lambda$. Figure 4 shows that the general rule of the reorganization energy decaying with increasing temperature extends to redox proteins with $\lambda \gg \lambda^{\rm St}$.

The largest entropy S_λ is observed for the variance reorganization energy λ, with $TS_\lambda/\lambda \simeq 0.5$ consistent with typical values observed for electron transfer in polar molecular liquids.[87] In contrast, the temperature variation of λ^r is significantly reduced, by an order of magnitude, due to the mutual cancellation of the corresponding temperature effects on $\lambda^{\rm St}$ and λ. This cancellation achieves a significant robustness of operation and insensitivity of the enzyme to the variations of thermodynamic conditions.[1] Consistently, a very small reaction entropy was recently reported for electrochemistry of immobilized myoglobin.[90]

Table 1: Reorganization parameters of Cyt-c at $T = 300$ K (eV).[a]

Parameter	λ	$\lambda^{\rm St}$	λ^r
λ	2.85	1.26	0.56
TS_λ	1.34	0.45	0.14

[a]The parameters in the Table are calculated from linear interpolations of the MD data in the range of temperatures from 280 K to 360 K (Figure 4).

The magnitude of λ^r, and its temperature dependence, are fully consistent with the experimental data. Figure 5 shows the temperature variation of $k_0 = k_c(0)$ measured for horse Cyt-c[33] immobilized on a self-assembled monolayer (SAM) on a metal electrode.[51,91,92] Immobilization is achieved by linking the heme of Cyt-C to terminal pyridine group of the PyC_{11}/C_{10} monolayer. The application of the

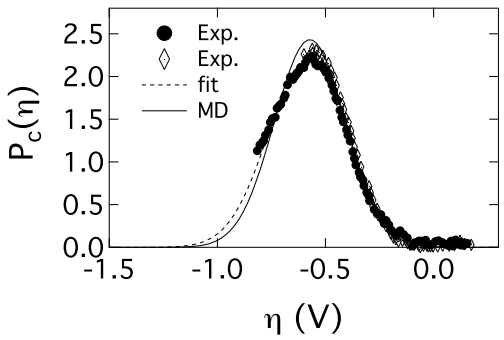

Figure 6: Normalized probability density $P_c(\eta)$ (eq 11) obtained from experiment with tuna (filled circles[30]) and horse (diamonds[31]) Cyt-c and from MD simulations (solid line). The experimental results were collected at $T = 273$ K from voltammograms with the electrode coated with the $OH-(CH_2)_{11}SH$ ω-hydroxyalkenthiol. The MD value of the reorganization energy $\lambda^r = 0.57$ eV was obtained by extrapolating the results shown in Figure 4 to 273 K. The dashed line is the Gaussian fit through the filled circles.

non-adiabatic electron-transfer rate requires the unknown parameter Δ in eq 10, which does not affect the slope of the Arrhenius plot ($\ln k_0$ vs $1/T$), but causes its vertical shift. The value of Δ was adjusted to fit the experimental data (points in Figure 5). A good agreement of the Arrhenius slope with experiment suggests that λ^r, and its temperature dependence, are reliably reproduced by the simulations. Neglecting the temperature dependence of λ^r results in a lower slope (dotted line), in accord with the positive sign of S_λ in Table 1 affecting the enthalpy of activation according to the relation

$$\Delta H^\dagger \simeq \frac{\lambda + TS_\lambda}{4} \qquad (19)$$

The estimate of the solvent dynamic effect,[62,64,65] with the relaxation time $\langle\tau\rangle \simeq 300-900$ ps obtained from simulations (see SI), shows that the term in the denominator in eq 12, containing $g \propto \langle\tau\rangle$ (eq 13), can be neglected for this reaction ($g \simeq 4\times10^{-4}$).

An independent test of our results is provided by voltammetry of horse Cyt-c performed[30] on an electrode coated with ω-hydroxyalkenthiol SAM of a thickness comparable to the one

used to produce data shown in Figure 5.[33] In these experiments, the derivative of the diffusion-corrected[41] electrode current $di_c/d\eta$ was recorded (points in Figure 6). As mentioned above, this derivative is proportional to the probability density $P_c(\eta)$ along the overpotential coordinate (eq 11). The probability density based on our MD simulations (solid line in Figure 6) is in good agreement with experiment without any additional fitting. The value of $\lambda^r \simeq 0.57$ eV used in the analysis is consistent with $\lambda^r \simeq 0.58 \pm 0.04$ eV reported previously[31,32] (native rat Cyt-c in Ref. 32).

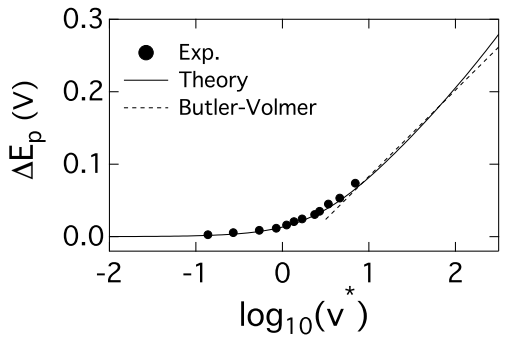

Figure 7: Shift of the cathodic peak potential ΔE_p vs the scan rate $\log_{10}(v^*)$, $v^* = ev/(k_{\rm B}Tk_c(0))$. The points are experimental data[33] and the solid line is the calculations[93,94] performed with $\lambda^r = 0.56$ eV and $\Delta = 2 \times 10^{-9}$ eV at $T = 298$ K. The dashed line indicates Laviron's[95] irreversible reaction limit with the slope $2.3k_BT/(\alpha e)$ and with the transfer coefficient $\alpha = 0.5$ (Butler-Volmer kinetics[50]).

Our results are also consistent with the reported cyclic voltammograms[33] without additional fitting (Figure 7). The calculations were performed by applying the rate constant as given by eq 10 to kinetic equations describing redox adsorbates (see SI).[93,94] The reorganization energy λ^r for the analysis is taken from our MD data and $\Delta = 2 \times 10^{-9}$ eV is the fitting parameter from the Arrhenius plot shown in Figure 5. The calculations are consistent with the expected limiting behavior for fully irreversible reactions where Laviron's solution[95] for the Butler-Volmer kinetics predicts the linear plot with the slope $2.3k_BT/(\alpha e)$ (dashed line in Figure 7 for the transfer coefficient $\alpha = 0.5$).

Discussion & Conclusions

Effective (reaction) reorganization energy λ^r (eq 2), combining the Stokes-shift and variance reorganization energies, controls the activation barrier of electrode electron transfer. The resulting low activation barrier is consistent with the values obtained from cyclic voltammograms. The low value of λ^r is specific to metalloproteins in solution. Here, we have not directly simulated the protein attached to the electrode and instead applied the results for the protein solution to interfacial electron transfer.

The effect of temperature on the activation barrier is significantly reduced compared to the standard models due to the compensation of individual temperature dependencies of λ and $\lambda^{\rm St}$ in λ^r. This result implies a robust operation of the redox enzyme, little affected by the alteration of temperature.

Redox enzymes act to lower the activation barrier for electron transfer. When the reaction free energy is low, lower barrier implies minimizing the reorganization energy (eq 8). It has been long anticipated that redox proteins should have evolved mechanisms to achieve this goal. However, traditional thinking in terms of a non-polar environment provided by the protein and producing low solvation energy turned out, with the help of atomistic simulations, to be inconsistent with a wet and covered with charges and polar groups environment of a typical redox site. The mechanisms which evolved in such a heterogenous environment appear to be different from the standard thinking of the Marcus model considering polarization of a homogeneous solvent in response to re-localizing the electron.

The heterogeneous protein-water thermal bath is capable of producing the spectrum of fluctuations deviating from the rules of the Gibbs ensemble by the fact of being trapped in non-equilibrium states on the time-scale of the reaction.[21] While this mechanism operates for a number of proteins, Cyt-c appears to be more stable and rigid than many other proteins, thus disallowing a large number of trap states. Polarizability of the active site is involved in

this case. It achieves the same result of an intense electrostatic noise effectively lowing the barrier for electron transfer. It appears that different mechanisms are involved with different proteins, all reaching the same goal of minimizing the reaction reorganization energy through large-amplitude interfacial noise. The principle of a noisy protein-water interface, also washing out small differences in thermodynamic conditions and effects of insignificant mutations, might be a general principle by which energy chains of biology achieve low activation barriers for physiological electron transport.

Supporting Information Available: Simulation protocols, additional data analysis, and derivation of equations used in the text. This material is available free of charge via the Internet at `http://pubs.acs.org/`.

Author Information:
Corresponding author: *`dmitrym@asu.edu`
Notes: The authors declare no competing financial interest.

Acknowledgement The authors acknowledge Hadi Dinpajooh and Daniel Martin for their help in setting up the simulations. David Waldeck provided us with experimental kinetic data. This research was supported by the National Science Foundation (CHE-1464810). CPU time was provided by the National Science Foundation through XSEDE resources (TG-MCB080071).

References

(1) Page, C. C.; Moser, C. C.; Chen, X. X.; Dutton, P. L. Natural engineering principles of electron tunneling in biological oxidation-reduction. *Nature* **1999**, *402*, 47–52.

(2) Gray, H. B.; Winkler, J. R. Long-range electron transfer. *Proc. Natl. Acad. Sci.* **2005**, *102*, 3534–3539.

(3) Skourtis, S. S.; Waldeck, D. H.; Beratan, D. N. Fluctuations in biological and bioinspired electron-transfer reactions. *Annu. Rev. Phys. Chem.* **2010**, *61*, 461–485.

(4) Marcus, R. A.; Sutin, N. Electron transfer in chemistry and biology. *Biochim. Biophys. Acta* **1985**, *811*, 265–322.

(5) Nicholls, D. G.; Ferguson, S. J. *Bioenergetics 3*; Academic Press: London, 2002.

(6) Gregory, R. B. In *Protein-solvent interactions*; Gregory, R. B., Ed.; Marcel Dekker: New York, 1995; p 191.

(7) Simonson, T. Electrostatics and dynamics of proteins. *Rep. Prog. Phys.* **2003**, *66*, 737–787.

(8) Warshel, A.; Sharma, P. K.; Kato, M.; Parson, W. W. Modeling electrostatic effects in proteins. *Biochim. Biophys. Acta* **2006**, *1764*, 1647–1676.

(9) Gabel, F.; Bicout, D.; Lehnert, U.; Tehei, M.; Weik, M.; Zaccai, G. Protein dynamics studied by neutron scattering. *Quat. Rev. Biophys.* **2002**, *35*, 327–367.

(10) Barlow, D. J.; Thornton, J. M. Charge distribution in proteins. *Biopolymers* **1986**, *25*, 1717–1733.

(11) Dill, K. A. Dominant forces in protein folding. *Biochemistry* **1990**, *29*, 7133–7155.

(12) Matyushov, D. V. Protein electron transfer: Dynamics and statistics. *J. Chem. Phys.* **2013**, *139*, 025102.

(13) Warshel, A. Dynamics of reactions in polar solvents. Semiclassical trajectory studies of electron-transfer and proton-transfer reactions. *J. Phys. Chem.* **1982**, *86*, 2218–2224.

(14) Horng, M. L.; Gardecki, J. A.; Papazyan, A.; Maroncelli, M. Subpicosecond measurements of polar solvation dynamics: Coumarin-153 revisited. *J. Phys. Chem.* **1995**, *99*, 17311–17337.

(15) Blumberger, J.; Klein, M. L. Reorganization free energies of long-range electron transfer in porphyrin-binding four-helix bundle protein. *J. Am. Chem. Soc.* **2006**, *128*, 13854–13867.

(16) Bortolotti, C. A.; Amadei, A.; Aschi, M.; Borsari, M.; Corni, S.; Sola, M.; Daidone, I. The Reversible Opening of Water Channels in Cytochrome c Modulates the Heme Iron Reduction Potential. *J. Am. Chem. Soc.* **2012**, *134*, 13670–13678.

(17) McCullagh, M.; Voth, G. A. Unraveling the role of the protein environment for [FeFe]-hydrogenase: A new application of coarse-graining. *J. Phys. Chem. B* **2013**, *117*, 4062–4071.

(18) Blumberger, J. Recent advances in the theory and molecular simulation of biological electron transfer reactions. *Chem. Rev.* **2015**, *115*, 11191–11238.

(19) LeBard, D. N.; Matyushov, D. V. Protein-water electrostatics and principles of bioenergetics. *Phys. Chem. Chem. Phys.* **2010**, *12*, 15335–15348.

(20) Heck, A.; Woiczikowski, P. B.; Kubar, T.; Giese, B.; Elstner, M.; Steinbrecher, T. B. Charge transfer in model peptides: obtaining Marcus parameters from molecular simulation. *J. Phys. Chem. B* **2012**, *116*, 2284–2293.

(21) Matyushov, D. V. Protein electron transfer: is biology (thermo)dynamic? *J. Phys.: Condens. Matter* **2015**, *27*, 473001.

(22) Reynolds, L.; Gardecki, J. A.; Frankland, S. J. V.; Maroncelli, M. Dipole solvation in nondipolar solvents: Experimental studies of reorganization energies and solvation dynamics. *J. Phys. Chem.* **1996**, *100*, 10337–10354.

(23) Matyushov, D. V.; Newton, M. D. Understanding the optical band shape: Coumarin-153 steady-state spectroscopy. *J. Phys. Chem. A* **2001**, *105*, 8516–8532.

(24) Small, D. W.; Matyushov, D. V.; Voth, G. A. The theory of electron transfer: What may be missing? *J. Am. Chem. Soc.* **2003**, *125*, 7470–7478.

(25) Dinpajooh, M.; Martin, D. R.; Matyushov, D. V. Polarizability of the active site of cytochrome *c* reduces the activation barrier for electron transfer. *Sci. Rep.* **2016**, *6*, 28152.

(26) Matyushov, D. V. Non-Gaussian statistics od binding/unbinding events and the energetics of electron transfer reactions. *Chem. Phys.* **2008**, *351*, 46–50.

(27) Vuilleumier, R.; Tay, K. A.; Jeanmairet, G.; Borgis, D.; Boutin, A. Extension of Marcus picture for electron transfer reactions with large solvation Changes. *J. Am. Chem. Soc.* **2012**, *134*, 2067–2074.

(28) Kuharski, R. A.; Bader, J. S.; Chandler, D.; Sprik, M.; Klein, M. L.; Impey, R. W. Molecular model for aqueous ferrous-ferric electron transfer. *J. Chem. Phys.* **1988**, *89*, 3248–3257.

(29) Blumberger, J.; Sprik, M. Quantum vs classical electron transfer energy as reaction coordinate for the aqueous Ru^{2+}/Ru^{3+} redox reaction. *Theor. Chem. Acc.* **2006**, *115*, 113–126.

(30) Terrettaz, S.; Cheng, J.; Miller, C. J. Kinetic parameters for cytochrome c via insulated electrode voltammetry. *J. Am. Chem. Soc.* **1996**, *118*, 7857–7858.

(31) Cheng, J.; Terrettaz, S.; Blankman, J. I.; Miller, C. J.; Dangi, B.; Guiles, R. D. Electrochemical comparison of heme proteins by insulated electrode voltammetry. *Israel J. Chem.* **1997**, *37*, 259–266.

(32) Wei, J. J.; Liu, H.; Niki, K.; Margoliash, E.; Waldeck, D. H. Probing electron tunneling pathways: Electrochemical study of rat heart cytochrome cand Its

mutant on pyridine-terminated SAMs. *J. Phy. Chem. B* **2004**, *108*, 16912–16917.

(33) Yue, H.; Khoshtariya, D.; Waldeck, D. H.; Grochol, J.; Hildebrandt, P.; Murgida, D. H. On the electron transfer mechanism between cytochrome *c* and Metal Electrodes. Evidence for Dynamic Control at Short Distances. *J. Phys. Chem. B* **2006**, *110*, 19906–19913.

(34) Alvarez-Paggi, D.; Castro, M. A.; Tórtora, V.; Castro, L.; Radi, R.; Murgida, D. H. Electrostatically driven second-sphere ligand switch between high and low reorganization energy forms of native cytochrome c. *J. Am. Chem. Soc.* **2013**, *135*, 4389–4397.

(35) Alvarez-Paggi, D.; Zitare, U.; Murgida, D. H. The role of protein dynamics and thermal fluctuations in regulating cytochrome c/cytochrome c oxidase electron transfer. *Biochim. Biophys. Acta - Bioenergetics* **2014**, *1837*, 1196–1207.

(36) Luz, R. A. S.; Crespilho, F. N. Gold nanoparticle-mediated electron transfer of cytochrome c on a self-assembled surface. *RSC Adv.* **2016**, *6*, 62585–62593.

(37) Chi, Q.; Zhang, J.; Andersen, J. E. T.; Ulstrup, J. Ordered assembly and controlled electron transfer of the blue copper protein azurin at gold (111) single-crystal substrates. *J. Phys. Chem. B* **2001**, *105*, 4669–4679.

(38) Jeuken, L. J. C.; McEvoy, J. P.; Armstrong, F. A. Insights into gated electron-transfer kinetics at the electrodeprotein interface: A square wave voltammetry study of the blue copper protein azurin. *J. Phys. Chem. B* **2002**, *106*, 2304–2313.

(39) Fedurco, M. Redox reactions of heme-containing metalloproteins: dynamic effects of self-assembled monolayers on thermodynamics and kinetics of cytochrome *c* electron-transfer reactions. *Coord. Chem. Rev.* **2000**, *209*, 263–331.

(40) Liu, J.; Chakraborty, S.; Hosseinzadeh, P.; Yu, Y.; Tian, S.; Petrik, I.; Bhagi, A.; Lu, Y. Metalloproteins containing cytochrome, iron–sulfur, or Copper Redox Centers. *Chem. Rev.* **2014**, *114*, 4366–4469.

(41) Becka, A. M.; Miller, C. J. Electrochemistry at .omega.-hydroxy thiol coated electrodes. 3. Voltage independence of the electron tunneling barrier and measurements of redox kinetics at large overpotentials. *J. Phys. Chem.* **1992**, *96*, 2657–2668.

(42) Fedurco, M.; Augustynski, J.; Indiani, C.; Smulevich, G.; Antalík, M.; Bánó, M.; Sedlák, E.; Glascock, M. C.; Dawson, J. H. Electrochemistry of unfolded cytochrome cin neutral and acidic urea solutions. *J. Am. Chem. Soc.* **2005**, *127*, 7638–7646.

(43) Waldeck, D. H.; Khoshtariya, D. E. *Applications of electrochemistry and nanotechnology in biology and medicine I*; Springer New York: New York, NY, 2011; pp 105–238.

(44) Warshel, A.; Weiss, R. M. An empirical valence bond approach for comparing reactions in solutions and in enzymes. *J. Am. Chem. Soc.* **1980**, *102*, 6218–6226.

(45) Warshel, A. *Computer modeling of chemical reactions in enzymes and solutions.*; Wiley Interscience: New York, 1991.

(46) Kubař, T.; Elstner, M. A hybrid approach to simulation of electron transfer in complex molecular systems. *J. R. Soc. Interface* **2013**, *10*, 20130415.

(47) Marcus, R. A. Relation between charge transfer absorption and fluorescence spectra and the inverted region. *J. Phys. Chem.* **1989**, *93*, 3078–3086.

(48) Mukamel, S. *Principles of nonlinear optical spectroscopy*; Oxford University Press: New York, 1995.

(49) Kubo, R. The fluctuation-dissipation theorem. *Rep. Prog. Phys.* **1966**, *29*, 255–284.

(50) Bard, A. J.; Faulkner, L. R. *Electrochemical methods. Fundamentals and applications*; Wiley: New York, 1980.

(51) Chidsey, C. E. D. Free energy and temperature dependence of electron transfer at the metal-electrolyte interface. *Science* **1991**, *251*, 919–922.

(52) Gorodyskii, A. V.; Karasevskii, A. I.; Matyushov, D. V. Adiabatic outer-sphere electron transfer through the metal-electrolyte interface. *J. Electroanal. Chem.* **1991**, *315*, 9–28.

(53) Straus, J. B.; Calhoun, A.; Voth, G. A. Calculation of solvent free energies for heterogeneous electron transfer at the water–metal interface: Classical versus quantum behavior. *J. Chem. Phys.* **1995**, *102*, 529–539.

(54) Schmickler, W. *Interfacial electrochemistry*; Oxford University Press: New York, 1996.

(55) VandeVondele, J.; Ayala, R.; Sulpizi, M.; Sprik, M. Redox free energies and one-electron energy levels in density functional theory based ab initio molecular dynamics. *J. Electroanal. Chem.* **2007**, *607*, 113–120.

(56) Koper, M. T. M. Combining experiment and theory for understanding electrocatalysis. *J. Electroanal. Chem.* **2005**, *574*, 375–386.

(57) Fleming, G. R.; Cho, M. Chromophore-solvent dynamics. *Annu. Rev. Phys. Chem.* **1996**, *47*, 109–134.

(58) Hush, N. S. Electron transfer in retrospect and prospect. 1: Adiabatic electrode processes. *J. Electroanal. Chem.* **1999**, *470*, 170–195.

(59) Migliore, A.; Nitzan, A. On the evaluation of the Marcus–Hush–Chidsey integral. *J. Electroanal. Chem.* **2012**, *671*, 99–101.

(60) Henstridge, M. C.; Laborda, E.; Rees, N. V.; Compton, R. G. Marcus–Hush–Chidsey theory of electron transfer applied to voltammetry: A review. *Electrochim. Acta* **2012**, *84*, 12–20.

(61) Schmickler, W. A theory of adiabatic electron-transfer reactions. *J. Electroanal. Chem.* **1986**, *204*, 31–43.

(62) Zusman, L. D. Outer-sphere electron transfer in polar solvents. *Chem. Phys.* **1980**, *49*, 295–304.

(63) Sumi, H.; Marcus, R. A. Dynamical effects in electron transfer reactions. *J. Chem. Phys* **1986**, *84*, 4894–4914.

(64) Rips, I.; Jortner, J. Dynamic solvent effects on outer-sphere electron transfer. *J. Chem. Phys.* **1987**, *87*, 2090–2104.

(65) Yan, Y. J.; Sparpaglione, M.; Mukamel, S. Solvation dynamics in electron-transfer, isomerization, and nonlinear optical processes: a unified Liouville-space theory. *J. Phys. Chem.* **1988**, *92*, 4842–4853.

(66) Morgan, J. D.; Wolynes, P. G. Adiabaticity of electron transfer at an electrode. *J. Phys. Chem.* **1987**, *91*, 874–883.

(67) Chakravarti, N.; Sebastian, K. L. Electrochemical electron transfer: a diffusion-reaction equation approach. *Chem. Phys. Lett.* **1992**, *193*, 456–460.

(68) Matyushov, D. Potential-step transient response of an electrochemical system. *J. Electroanal. Chem.* **1994**, *367*, 1–6.

(69) van der Zwan, G.; Hynes, J. T. Time-dependent fluorescence solvent shifts, dielectric friction, and nonequilibrium solvation in polar solvents. *J. Phys. Chem.* **1985**, *89*, 4181.

(70) Maroncelli, M. The dynamics of solvation in polar liquids. *J. Mol. Liq.* **1993**, *57*, 1–37.

(71) Pierce, D. W.; Boxer, S. G. Dielectric relaxation in a protein matrix. *J. Phys. Chem.* **1992**, *96*, 5560–5566.

(72) Jordanides, X. J.; Lang, M. J.; Song, X.; Fleming, G. R. Solvation dynamics in protein environments studied by photon echo spectroscopy. *J. Phys. Chem. B* **1999**, *103*, 7995–8005.

(73) Lampa-Pastirk, S.; Beck, W. F. Polar solvation dynamics in Zn(II)-substituted cytochrome c: Diffusive sampling of the energy landscape in the hydrophobic core and solvent-contact layers. *J. Phys. Chem. B* **2004**, *108*, 16288–16294.

(74) Qin, Y.; Jia, M.; Yang, J.; Wang, D.; Wang, L.; Xu, J.; Zhong, D. Molecular origin of ultrafast water–Protein coupled interactions. *J. Phys. Chem. Lett.* **2016**, *7*, 4171–4177.

(75) Phillips, J. C.; Braun, R.; Wang, W.; Gumbart, J.; Tajkhorshid, E.; Villa, E.; Chipot, C.; Skeel, R. D.; Kalé, L.; Schulten, K. Scalable molecular dynamics with NAMD. *J. Comput. Chem.* **2005**, *26*, 1781–1802.

(76) Marcus, R. A. Electrostatic free energy and other properties of states having nonequilibrium polarization. I. *J. Chem. Phys.* **1956**, *24*, 979–989.

(77) Dinpajooh, M.; Matyushov, D. V. Interfacial structural transition in hydration shells of a polarizable solute. *Phys. Rev. Lett.* **2015**, *114*, 207801.

(78) Dinpajooh, M.; Newton, M. D.; Matyushov, D. V. Free energy functionals for polarization fluctuations: Pekar factor revisited. *J. Chem. Phys.* **2017**, *145*, 064504.

(79) Matyushov, D. V.; Newton, M. D. Solvent-induced shift of spectral lines in polar-polarizable solvents. *J. Phys. Chem. A* **2017**, acs.jpca.7b00414–9.

(80) Gupta, S.; Matyushov, D. V. Solvent and solute polarizability effects on the reorganization energy of electron transfer. *J. Phys. Chem. A* **2004**, *108*, 2087–2096.

(81) Milischuk, A. A.; Matyushov, D. V.; Newton, M. D. Activation entropy of electron transfer reactions. *Chem. Phys.* **2006**, *324*, 172–194.

(82) Liu, W.; Rumbley, J. N.; Englander, S. W.; Wand, A. J. Fast structural dynamics in reduced and oxidized cytochrome c. *Protein Science* **2009**, *18*, 670–674.

(83) Sigfriddson, E.; Olsson, M. H. M.; Ryde, U. A comparison of the inner-sphere reaorganization energies of cytochromes, iron-sulfur clusters, and blue copper proteins. *J. Phys. Chem. B* **2001**, *105*, 5546–5552.

(84) Amashukeli, X.; Gruhn, N. E.; Lichtenberger, D. L.; Winkler, J. R.; Gray, H. B. Inner-sphere electron-transfer reorganization energies of zinc porphyrins. *J. Am. Chem. Soc.* **2004**, *126*, 15566–15571.

(85) Cascella, M.; Magistrato, A.; Tavernelli, I.; Carloni, P.; Rothlisberger, U. Role of protein frame and solvent for the redox properties of azurin from *Pseudomonas aeruginosa*. *Proc. Natl. Acad. Sci.* **2006**, *103*, 19641–19646.

(86) Bixon, M.; Jortner, J. Electron transfer – from isolated molecules to biomolecules. *Adv. Chem. Phys.* **1999**, *106*, 35.

(87) Ghorai, P. K.; Matyushov, D. V. Solvent reorganization entropy of electron transfer in polar solvents. *J. Phys. Chem. A* **2006**, *110*, 8857–8863.

(88) Waskasi, M. M.; Gerdenis,; Moore, A. L.; Moore, T. A.; Gust, D.; Matyushov, D. V. Marcus bell-shaped electron transfer kinetics observed in an Arrhenius plot. *J. Am. Chem. Soc.* **2016**, *138*, 9251–9257.

(89) Vath, P.; Zimmt, M. B.; Matyushov, D. V.; Voth, G. A. A failure of continuum theory: Temperature dependence of the solvent reorganization energy of electron transfer in highly polar solvents. *J. Phys. Chem. B* **1999**, *103*, 9130–9140.

(90) Khoshtariya, D. E.; Dolidze, T. D.; Shushanyan, M.; van Eldik, R. Long-range electron transfer with myoglobin immobilized at Au/mixed-SAM junctions: Mechanistic impact of the strong protein confinement. *J. Phys. Chem. B* **2014**, *118*, 692–706.

(91) Smalley, J. F.; Sachs, S. B.; Chidsey, C. E. D.; Dudek, S. P.; Sikes, H. D.; Creager, S. E.; Yu, C. J.; Feldberg, S. W.; Newton, M. D. Interfacial electron-transfer kinetics of ferrocene through oligophenyleneethynylene bridges attached to gold electrodes as constituents of self-assembled monolayers: Observation of a nonmonotonic distance dependence. *J. Am. Chem. Soc.* **2004**, *126*, 14620–14630.

(92) Newton, M. D.; Smalley, J. F. Interfacial bridge-mediated electron transfer: mechanistic analysis based on electrochemical kinetics and theoretical modelling. *Phys. Chem. Chem. Phys.* **2007**, *9*, 555–572.

(93) Nahir, T. M.; Clark, R. A.; Bowden, E. F. Linear-sweep voltammetry of irreversible electron transfer in surface-confined species using the Marcus theory. *Anal. Chem.* **1994**, *66*, 2595–2598.

(94) Honeychurch, M. J. Effect of electron-transfer rate and reorganization energy on the cyclic voltammetric response of redox adsorbates. *Langmuir* **1999**, *15*, 5158–5163.

(95) Laviron, E. General expression of the linear potential sweep voltammogram in the case of diffusionless electrochemical system. *J. Electroanal. Chem.* **1979**, *101*, 19–28.

Figure Legends

Figure 1 (a) Reaction coordinate $X = \hbar\omega$ for solution electron transfer between the donor (D) and acceptor (A).[13] (b) Probability densities for absorbing (abs.) and emitting (em.) a photon in a charge-transfer optical transition; $\langle X\rangle_i$ stand for the average transition energies. The separation between the peaks of optical transitions represents the Stokes shift and the corresponding reorganization energy λ^{St}. (c) The free energy surfaces of electron transfer $G_i(X) = G_0^i - k_{\mathrm{B}}T\ln[P_i(X)]$ following from the optical transition probabilities $P_i(X)$. The reorganization energy λ defines the curvature of the free energy surface near the bottom (shown by the double arrow). It also provides the measure of inhomogeneous broadening of the optical charge-transfer band[14] ($\sigma_X^2 = \langle(\delta X)^2\rangle = 2k_{\mathrm{B}}T\lambda$ in (b) and in eq 3). The filled dots in (b) and (c) indicate, respectively, $P_2(0)$ and the crossing point of $G_i(X)$ representing the transition state, $X = 0$, of the electron-transfer reaction.

Figure 2 Schematics of cathode electron transfer from the Fermi energy level ϵ_F, corresponding to the equilibrium electrode potential, to an oxidized reactant with the average energy ϵ_{Ox}. Electron transfer predominantly occurs from ϵ_F to a nonequilibrium energy level in resonance with it with the electrode-reactant electronic coupling Δ (eq 10). The nonequilibrium energy level is a part of a Gaussian manifold with the variance $\sigma^2 = 2k_BT\lambda$ specifying the reorganization energy λ (eq 3). The overpotential η shifts the electrode chemical potential as $\mu = \epsilon_F - e\eta$.

Figure 3 Quantum center of Cyt-c used in the calculations to compute the Hamiltonian matrix in eq 16. It includes the heme (gray, with Fe colored red), histidine (blue), methionine (green), and two cysteine (orange) amino acids.

Figure 4 Temperature dependence of reorganization energies from QM/MD simulations. Shown separately are the variance reorganization energies λ_i (eq 3) in the reduced (red diamonds) and oxidized (blue triangles) states of Cyt-c and their mean values (black circles). Squares refer to the Stokes-shift reorganization energy λ^{St} (eq 7) and black diamonds refer to the reaction reorganization energy λ^r (eq 2). The dashed lines are linear regressions through the simulation points (the upper dashed line is a linear regression through the mean values $\lambda(T)$).

Figure 5 Rate constant $k_0 = k_c(0)$ (eq 10) at $\eta = 0$ for horse Cyt-c on the gold electrode modified with $\mathrm{PyC_{11}/C_{10}}$ self-assembled monolayer[33] (points, Exp.). The solid line shows the calculations based on eqs 10 and 12, which give identical results. The electron coupling $\Delta = 2\times 10^{-9}$ eV is used to reproduce the experimental data. The temperature-dependent reorganization energy $\lambda^r(T)$ from Figure 4 was used in eqs 10 and 12. The dotted line shows the result of neglecting the temperature dependence $\lambda^r(T)$ and putting $\lambda^r = \lambda^r(300\ \mathrm{K})$.

Figure 6 Normalized probability density $P_c(\eta)$ (eq 11) obtained from experiment with tuna (filled circles[30]) and horse (diamonds[31]) Cyt-c and from MD simulations (solid line). The experimental results were collected at $T = 273$ K from voltammograms with the electrode coated with the $\mathrm{OH-(CH_2)_{11}SH}$ ω-hydroxyalkenthiol. The MD value of the reorganization energy $\lambda^r = 0.57$ eV was obtained by extrapolating the results shown in Figure 4 to 273 K. The dashed line is the Gaussian fit through the filled circles.

Figure 7 Shift of the cathodic peak potential ΔE_p vs the scan rate $\log_{10}(v^*)$, $v^* = ev/(k_{\mathrm{B}}Tk_c(0))$. The points are experimental data[33] and the solid line is the calculations[93,94] performed with $\lambda^r = 0.56$ eV and $\Delta = 2\times 10^{-9}$ eV at $T = 298$ K. The dashed line indicates Laviron's[95] irreversible reaction limit with the slope $2.3k_BT/(\alpha e)$ and with the transfer coefficient $\alpha = 0.5$ (Butler-Volmer kinetics[50]).

Graphical TOC Entry